Nanoscience and Nanotechnology Letters
Vol. 4, 1074–1081, 2012

Double-Wall Carbon Nanotubes of Different Morphology: Electronic Structure Simulations

Yuri F. Zhukovskii[1,*], Sergei Piskunov[1,2,3], and Stefano Bellucci[4]

[1] *Institute of Solid State Physics, University of Latvia, Kengaraga Street 8, LV-1063 Riga, Latvia*
[2] *Faculty of Computing, University of Latvia, Raina Boulevard 19, LV-1586 Riga, Latvia*
[3] *Faculty of Physics and Mathematics, University of Latvia, Zellu Street 8, LV-1002 Riga, Latvia*
[4] *INFN-Laboratori Nazionali di Frascati, Via Enrico Fermi 40, I-00044, Frascati (Rome), Italy*

Double-wall (DW) CNTs consisting of two coaxial single-wall (SW) constituents, possess mechanical, structural and electronic properties which are superior to SW CNTs. DW CNT is also the simplest model of multi-wall (MW) carbon nanotube. In this study, we have simulated DW NTs with not only commensurate (6, 6)@(11, 11) and (10, 0)@(19, 0) morphologies (analogously to those double-wall carbon nanotubes studied so far), but also incommensurate (6, 6)@(19, 0) and (10, 0)@(11, 11) ones, all described by asymmetric *P*1 rod group. Inter-shell distances in aforementioned nanotubes are changed from 3.37 to 3.54 Å, within the interval of DW CNT stability. Due to essential difference between the translation periods of SW CNTs with (n_1, n_1) and $(n_2, 0)$ chirality indices (their ratio is $1/\sqrt{3}$), we have been able to use the first-principles DFT-LCAO method only for detailed calculations on the first two nanotube configurations mentioned above (using unit cell model), while the semi-empirical self-consistent-charge density-functional tight-binding (SCC-DFTB) method has been applied for calculations of all four DW NT configurations (in the framework of supercell model characterized by large translation length unit of incommensurate double-wall nanotube achieving 4.24 nm). Combining both methods for calculations on SW and DW CNTs, we have analyzed their electronic properties (e.g., band structure, density of states as well as electronic charge redistribution).

Keywords: Morphology of DW CNTs, *Ab Initio* DFT-LCAO Method, Semi-Empirical SCC-DFTB Method, Calculated Parameters of CNT Electronic Structure.

1. INTRODUCTION

Broad technological application of carbon nanotubes (CNTs) is still hindered by inability to provide reproducible growth of CNTs with predetermined chirality indices since existing experimental methods of nanotube synthesis yield a mixture of metallic and semiconducting nanotubes.[1–3] Multi-wall (MW) nanotubular structures were found to be grown more efficiently as compared to SW NTs with diameters > 1.5–2.0 nm.[4] Since MW CNTs contain a few concentric nanotubular shells, they have more complex electronic and transport properties as compared to SW CNTs, mainly due to the inter-wall interactions between the adjacent shells.[2,3] A number of quantum effects, such as the ballistic transport, the negative magnetoresistance and the interference effect, have been observed in MW CNTs.[5] On the other hand, the propagation of azimuthally symmetric guided waves inside the multi-walled carbon nanotubes, which is technologically important for the electromagnetic characteristics of CNT-based antennas, was recently analyzed theoretically.[6] When modeling the electromagnetic properties of an MW CNT, the inter-wall interaction leading to either electron tunneling or hopping between the shells is one of critical points for a proper description of aforementioned propagation effects.[6,7]

The simplest examples of MW CNTs are coaxial double-wall nanotubes (DW CNTs) which provide rational explanation for the dependence of their electronic and structural properties on the inter-wall van der Waals-type interactions.[8] The two-shell structure can protect the inner tube from the external perturbations, thus giving the desired properties of nanotube cables, field-effect transistors and molecular capacitors.[3] DW CNTs with outer diameter ~1.5 nm were synthesized by fusion of fullerenes encapsulated in SW NTs.[9,10]

A number of theoretical simulations on equilibrium structure and electronic properties of commensurate DW CNTs were performed so far.[5,8,11–17] For majority of

*Author to whom correspondence should be addressed.

 1941-4900/2012/4/1074/008 doi:10.1166/nnl.2012.1460

these calculations, the plane-wave formalism of Density Functional Theory (DFT-PW) was applied, within the Local Density Approximation (LDA), in order to simulate DW NTs possessing armchair-type (*ac*-)[8] or zigzag-type (*zz*-),[11,16] and both types of chiralities.[13,17] The linearized augmented cylindrical-wave (LACW) method[14] was also developed for DFT-LDA calculations on both *ac*- and *zz*-chiralities of any DW NTs. In recent *ab initio* DFT + HF hybrid calculations on the atomic structure and electronic properties of commensurate BN and TiO_2 DW NTs with hexagonal morphology using the Generalized Gradient Approximation (GGA), we have applied the formalism of linear combination of localized atomic functions (LCAO).[18] The LCAO formalism (within LDA approach) was also used for construction of both Hamiltonian and overlap matrices for further generation of Green's functions, necessary to estimate conductance in DW CNTs.[15] Semi-empirical tight-binding (TB) method was applied for calculations of both electronic[5,15] and phonon[12] properties of DW NTs, while atomistic method based on the Lennard-Jones potential served for determination of equilibrium structures of various double-wall nanotubes with arbitrary chiralities.[12]

The energetically most stable configurations among the commensurate DW CNTs with *ac*- and *zz*-chiralities were found to be $(6,6)@(11,11)$ and $(9,0)@(18,0)$, respectively, with the inter-shell spacing 3.4–3.6 Å (as to chiral double-wall nanotubes, they were found to be less stable).[17] Moreover, for the two series of DW CNTs studied within the diameter range, the most stable inner-outer combination is consistently $(n_1,n_1)@(n_1+5,n_1+5)$ for armchair pairs and $(n_2,0)@(n_2+9,0)$ for zigzag pairs.[13] One of the top questions for DW CNTs solved using their theoretical simulations is the inter-shell interaction and its influence on the electronic properties. In the symmetric DW configurations consisting of two metallic shells (when $|n_1-n_2|$ is a multiple of three), energy bands crossed near the Fermi level ε_F.[8] In the asymmetric case, band crossing is not allowed at all, causing the formation of pseudo-gaps in the density of states. While the inter-shell hybridization opens up pseudo-gaps in the electronic structure, it modifies the character of the corresponding wave function near ε_F, and hence is likely to affect the conductivity of multi-wall nanotubes. On the other hand, semiconducting $(n_1,0)@(n_2,0)$ CNTs keep a smaller band gap as compared to that of inner or outer tubes.[16]

Another aspect of the inter-shell interaction in DW CNTs is a charge transfer between the two weakly interacting SW shells which can be correlated with the difference of their work functions.[8] At the same time, the inter-shell interaction in the multi-wall tubes is not so weak, to allow the extrapolation of work functions for the isolated single-wall tubes. The predicted work function variation of double-wall CNTs indicated a potential difficulty

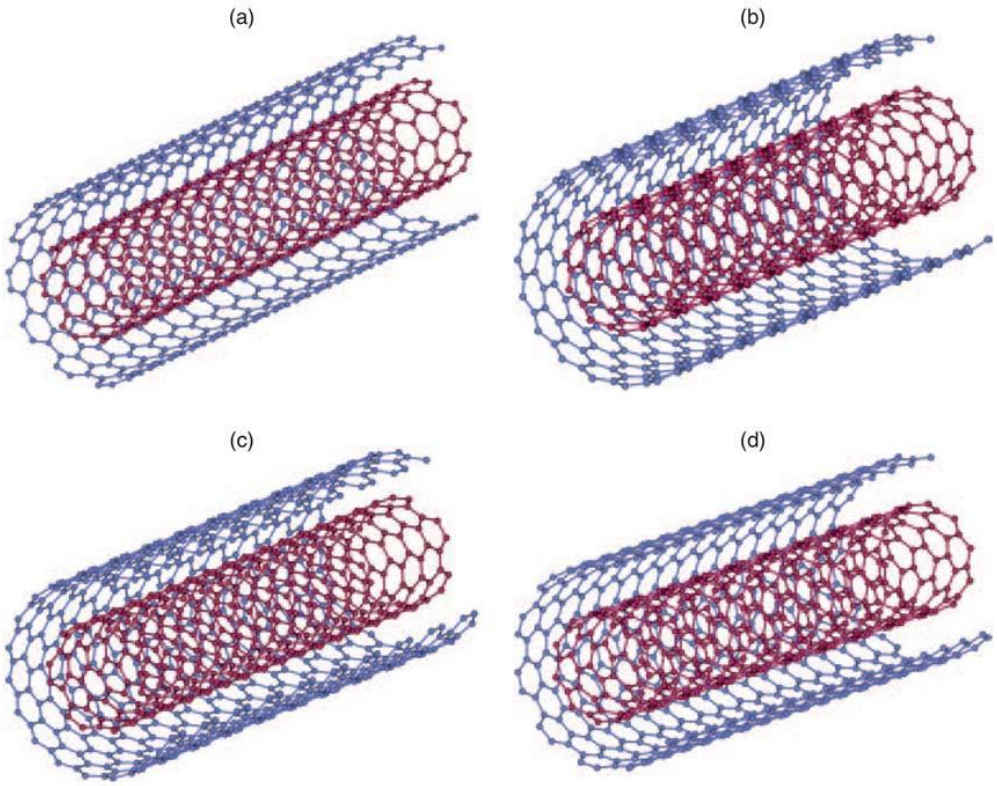

Fig. 1. Models of coaxial $(6,6)@(11,11)$ (a), $(10,0)@(19,0)$ (b), $(6,6)@(19,0)$ (c) and $(10,0)@(11,11)$ (d) DW CNTs as simulated in the current study.

in their nanoelectronic device applications.[13] Judging from very similar charge redistributions found for the symmetric and asymmetric DW CNTs, the chirality and diameter of the individual nanotubes matter more than relative nanotube orientations.[11] It was rather problematic to pinpoint the dominant eigenstates responsible for the charge transfer into the inter-shell region, since the charge redistribution is contributed from many eigenstates, some of them are far below ε_F. There appears to be a significant hybridization between these deep states and the inter-shell state.

In this paper, we analyze results of: (i) DFT-LCAO calculations on the commensurate $(6,6)@(11,11)$ and $(10,0)@(19,0)$ CNTs, as well as (ii) self-consistent-charge density-functional tight-binding (SSC-DFTB) calculations both on pair of commensurate nanotubes mentioned above and, for the first time, on pair of incommensurate $(6,6)@(19,0)$ and $(10,0)@(11,11)$ nanotubes. Section 2 shortly describes basic concepts of DFT-LCAO and SSC-DFTB methods. In Section 3, we consider asymmetric models of both commensurate and incommensurate DW CNTs (Fig. 1). In the former case, we apply the unit cell model (the same as for SW CNTs), while in the latter case, we use the supercell model characterized by large translation length unit (4.24 nm). Combining both methods for calculations on SW and DW CNTs, we analyze and compare in Section 4 their electronic properties.

2. COMPUTATIONAL DETAILS

2.1. DFT-LCAO Method

The first-principles DFT and Hartree-Fock (HF) methods, as implemented in the *CRYSTAL*-09 code,[19] are based on the self-consistent field (SCF) solution of the one-electron equations:

$$\hat{h}_i \varphi_{\mathbf{k}i}(\mathbf{r}) = \varepsilon_{\mathbf{k}i} \varphi_{\mathbf{k}i}(\mathbf{r}) \tag{1}$$

where crystalline orbitals $\varphi_{\mathbf{k}i}(\mathbf{r})$ of the N-electron system (per unit cell) are expanded as linear combinations of the set of m Bloch functions built from the local, atom-centered Gaussian-type functions (GTFs):

$$\varphi_{\mathbf{k}i}(\mathbf{r}) = N \sum_{j=1}^{m} a_{ij}(\mathbf{k}) \left(\sum_{\mathbf{g}} \chi_{\mathbf{g}j}(\mathbf{r}) \exp(i\mathbf{k}\cdot\mathbf{g}) \right) \tag{2a}$$

$$\chi_{\mathbf{g}j}(\mathbf{r}-\mathbf{R}_j) = \sum_{\mu}^{n_G} c_\mu G(\alpha_\mu; \mathbf{r}-\mathbf{R}_j-\mathbf{g}) \tag{2b}$$

where $\mathbf{k}$ is the wave vector of the irreducible representation of the group of crystal translations $\{\mathbf{g}\}$; $\mathbf{R}_j$ denotes the coordinates of nuclei in the zero cell of which the atomic orbital $\chi_{gj}(\mathbf{r})$ is centered; G, c_μ and α_μ are the normalized GTFs, its coefficients and exponents, respectively. In the current study, we have used the all-valence basis set (BS) of GTFs for carbon atom in the form (6*s*-311*sp*-11*d*) suggested in *CRYSTAL* Manual,[19] with further re-optimization.

The DFT-LCAO method allows us to describe nanotubes in their original 1D space form, unlike the PW methods, which were used mainly for *ab initio* calculations on DW CNTs. Indeed, to restore the 3D periodicity in the PW nanotube calculations, the x–y supercell of nanotubes is artificially introduced:[18] the NTs are placed into a square array with the inter-tube distance up to 3 nm. At such separations, the inter-wall interaction is usually found to be rather small, however, the convergence of results obtained using such a PW calculations depends on the artificial inter-tube interactions (thus, the additional computational efforts should be provided to ensure their negligibility). Such an artifact is certainly absent for description of 1D nanostructures when using LCAO formalism.

Various types of DFT-LCAO method, as implemented in *CRYSTAL*-09 code,[19] differ by the exchange-correlation functionals:

$$\hat{v}_{xc} = \frac{\partial E_{xc}[\rho(\mathbf{r}); \mathbf{k}]}{\partial \rho(\mathbf{r})} \tag{3}$$

where E_{xc} is the energy functional while $\rho(\mathbf{r})$ the electron density function. The GGA-corrected exchange-correlation functional by Perdew, Burke and Ernzerhof (PBE)[20] has been used in our spin-polarized calculations. To provide a balanced summation in both direct and reciprocal lattices, the reciprocal space integration has been performed by sampling the Brillouin zone with the $8 \times 1 \times 1$ Pack-Monkhorst mesh[19] which results in 5 k-points in total for unit cell of SW and DW CNTs. Calculations are considered as converged only when the total energy differs by less than 10^{-7} a.u. in two successive cycles of the self-consistency procedure. A smearing temperature of 0.001 a.u. has been applied to the Fermi function.[19] This value has been chosen relatively low, to ensure that the magnetic moment is not artificially modified by a too high value. All the calculations have been performed with the total geometry optimization.

2.2. SSC-DFTB Method

The DFTB method is based on a second-order expansion of the Kohn-Sham total energy within DFT approach, with respect to charge density fluctuations.[21] The 0th-order approach is equivalent to a common standard non-self-consistent semi-empirical TB scheme,[22] while at second order a transparent, parameter-free, and readily calculable expression for the generalized Hamiltonian matrix elements can be derived. These are modified by a self-consistent redistribution of Mulliken charges (SCC). Besides the usual band structure and short-range repulsive terms the final approximate Kohn-Sham energy within the DFTB method additionally includes a Coulomb interaction between the charge fluctuations. This accounts for long-range electrostatic forces at large distances between the two point charges and approximately includes self-interaction contributions of a given atom if the charges are located at one and the same atom. Due to the SCC

extension, the DFTB method can be successfully applied to problems, where deficiencies within the non-SCC standard Slater-Koster TB approach[22] become obvious.

The total DFTB energy within the spin-polarized approach (SDFTB) is present as a sum of four terms:[21]

$$E_{tot}^{SDFTB} = \sum_{\sigma=\uparrow,\downarrow}\sum_{i}^{occ} n_{i\sigma}\langle\psi_{i\sigma}|\hat{H}^0[n_0]|\psi_{i\sigma}\rangle + \frac{1}{2}\sum_{\alpha\beta}^{N}\gamma_{\alpha\beta}\Delta q_\alpha \Delta q_\beta + \frac{1}{2}\sum_{\alpha}^{N}\sum_{l\in\alpha}\sum_{l'\in\alpha} p_{\alpha l}p_{\alpha l'}W_{\alpha ll'} + E_{rep} \quad (4)$$

where spin populations in different spin states are expressed via Mulliken populations ($p_{\alpha l} = q_{\alpha l\uparrow} - q_{\alpha l\downarrow}$):

$$q_{\alpha i\sigma} = \frac{1}{2}\sum_{i}^{occ} n_{i\sigma}\sum_{\mu\in l\alpha}\sum_{\nu}^{N}(c^*_{\mu i\sigma}c_{\nu i\sigma}S_{\mu\nu} + c^*_{\nu i\sigma}c_{\mu i\sigma}S_{\nu\mu}) \quad (5)$$

Variation of approximate Kohn-Sham energy expression, Eq. (4), with respect to the minimal basis yields single-particle 'Kohn-Sham-like' equations:

$$\sum c_{\nu i\alpha}(H_{\mu\nu\alpha} - \varepsilon_{i\sigma}S_{\mu\nu}) = 0 \quad \forall\mu, i, \sigma \quad (6)$$

Values of $n_{i\sigma}$ and n_0 describe spin-polarized and reference densities, respectively, $H_{\mu\nu\alpha}$ and $S_{\mu\nu}$ are elements of Hamiltonian and overlap matrices, while $\psi_{i\sigma}$ are optimized pseudo-atomic orbitals. Constants $W_{\alpha ll'}$ are resolved with respect to the angular momentum, while $\gamma_{\alpha\beta}$ are determined analytically from the Coulomb interaction of two atom-centered spherical charge distributions located at $\boldsymbol{R}_\alpha$ and $\boldsymbol{R}_\beta$. The short-range repulsive energy E_{rep} is defined from the specific atom-type pair potentials $U(\boldsymbol{R}_{\alpha\beta})$.

When using the DFTB method, the Slater-Koster file for description of C–C interaction was obtained from the DFT-PBE calculations on diamond.[23] Experimental cell constant was reproduced in this case within ~2 per cent.

One of the most noticeable advantages of SSC-DFTB method is the size of periodic unit which can be calculated: the maximum number of atoms per supercell describing by asymmetric $P1$ rod group is 1500–2000 versus 150–200 atoms per supercell when performing analogous DFT-LCAO calculations (i.e., total number is about ten times larger).

3. MODELS OF DW CNTs

The four DW CNTs with different chirality combinations, i.e., (6, 6)@(11, 11), (10, 0)@(19, 0), (6, 6)@(19, 0), and (10, 0)@(11, 11), have been simulated in this study (Fig. 1). Due to difference of translation periods for SW CNTs with (n_1, n_1) and $(n_2, 0)$ chirality indices by irrational number of times ($\sqrt{3}$), only the first two DW NT configurations from those mentioned above can be calculated using first-principles DFT-LCAO method.[19] Indeed, (6, 6)@(11, 11), (10, 0)@(19, 0) nanotubes contain 68 and 116 atoms per DW CNT unit cell, respectively. At the same time, *CRYSTAL*-09 code restricts the number of basic functions by 10000;[17] since BS of C mentioned in Subsection 2.1 contains 23 GTFs while graphene unit cell consists of two carbon atoms, the computational limit of atoms per asymmetric DW NT unit cell is 10000/46 ≈ 217.

Table I. Three types of nanotube combinations used for DFTB calculations on commensurate and incommensurate DW CNTs shown in Figure 1. Values of N_{DW} describe numbers of atoms per DW NTs, $d_{ac} = 2.473$ Å and $d_{zz} = 4.282$ Å are unit lengths of *ac*- and *zz*-shells, while Δ_{ac-zz} and δ_{ac-zz} are absolute and relative errors of averaged unit lengths for incommensurate DW CNTs.

	$9d_{ac}$@$5d_{zz}$		$17d_{ac}$@$10d_{zz}$		$26d_{ac}$@$15d_{zz}$	
Model	N_{DW}	Δ_{ac-zz} (Å) (δ_{ac-zz}, %)	N_{DW}	Δ_{ac-zz} (Å), (δ_{ac-zz}, %)	N_{DW}	Δ_{ac-zz} (Å), (δ_{ac-zz}, %)
Figure 1(a)*	612	–	1156	–	1768	–
Figure 1(b)*	580		1160		1740	
Figure 1(c)	596	0.83	1168	0.39	1764	0.03
Figure 1(d)	596	(3.556)	1148	(0.943)	1744	(0.037)

Note: *Morphology of commensurate DW NTs corresponds to that of the constituent SW NTs with a length of supercell exceeding parameter of unit cell by the corresponding number of times as described in the upper row of table.

On the other hand, to determine a number of supercells per *ac* and *zz* shells of incommensurate DW CNTs supercells, which ratio approaches to $\sqrt{3} \approx 1.73205$, we have considered different possible nanotube combinations with different levels of precision (Table I). For each DW NT pattern, we have estimated absolute and relative differences between the lengths of *ac*- ad *zz*-supercells via their stretch or compression with regards to arithmetic average (Δ_{ac-zz} and δ_{ac-zz}, respectively). When considering DW combination $9d_{ac}$@$5d_{zz}$, the value of δ_{ac-zz} is found to be inadmissibly large (3.66 per cent), while for $26d_{ac}$@$15d_{zz}$, with almost neglecting δ_{ac-zz} (0.04 per cent) the total number of atoms in DW NT supercells (N_{DW}) exceeds restriction of the DFTB code.[21] This is why we have chosen for simulation of incommensurate DW CNTs $17d_{ac}$@$10d_{zz}$ recalculating commensurate DW CNTs too.

4. RESULTS AND DISCUSSION

4.1. DFT-LCAO and DFTB Calculations on SW CNTs

The simplest verification of the electronic structure calculated using *ab initio* DFT-LCAO and semi-empirical DFTB methods has been achieved for the band structures of SW CNTs corresponding to constituents of DW CNTs (Fig. 1) of either *ac*- or *zz*-chiralities (Figs. 2(a), (b)). Comparison of DFT-LCAO and DFTB band structures clearly shows their qualitative similarity, especially below the Fermi level, and confirms existence of direct gap for *zz*-CNT.[11]

The tight-binding energetic parameter $\gamma_0 = 2.17$ eV was taken to match the band-gap calculated using

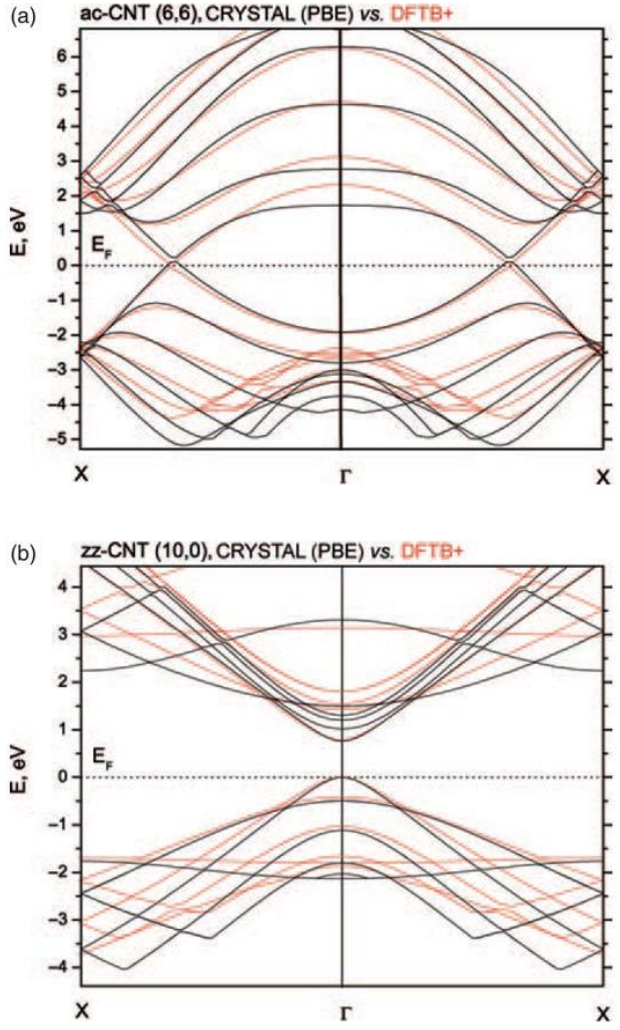

Fig. 2. Band structures for $(6,6)$ (a) and $(10,0)$ (b) SW CNTs are shown according to calculations performed using both DFT-LCAO (black solid lines) and DFTB (red dashed lines) methods.

DFT-LCAO method for the semiconducting $(10,0)$ nanotube (Fig. 2(b)):

$$E_{\pm}(\mathbf{k}) = \pm\gamma_0\sqrt{4\cos^2\frac{k_y d}{2} + 4\cos\frac{\sqrt{3}k_x d}{2}\cos\frac{k_y d}{2} + 1} \quad (7)$$

where d is a period of zz-SW CNT, while k_x and k_y are projections of **k**-vector for nanotube in the reciprocal space.

4.2. Comparison of DFT-LCAO and DFTB Structural and Total Energy Parameters of DW CNTs

In Table II, we compare initial and optimized geometry parameters (diameter of inner shell D_{NT}^{in} as well as inter-shell distance ΔR_{NT}) calculated using both methods and present the corresponding relaxation energies per carbon atom (E_{relax}). Obviously, the latter have been found to be substantially larger when performing DFTB calculations, especially on incommensurate DW CNTs (Table II).

Table II. Structural properties of DW CNTs calculated using DFT-LCAO and DFTB methods. For commensurate DW NTs, both methods have been applied while incommensurate nanotubes have been calculated within DFTB approach. Values of ΔR_{NT}, D_{NT}^{in} and E_{relax} are defined above.

		ΔR_{NT} (Å)		D_{NT}^{in} (Å)		E_{relax}
Model	Method	Initial	Optimized*	Initial	Optimized*	(eV/at)
Figure 1(a)	DFT-LCAO	3.39	3.38	8.12	8.14	0.005
	DFTB		3.37		8.15	0.008
Figure 1(b)	DFT-LCAO	3.53	3.53	7.84	7.85	0.002
	DFTB		3.52		7.87	0.011
Figure 1(c)	DFTB	3.37	3.40	8.12	8.11	0.055
Figure 1(d)	DFTB	3.54	3.52	7.84	7.85	0.063

Note: *Averaged values.

Moreover, we have estimated the binding energy between shells of commensurate $(6,6)@(11,11)$ CNT (which was found to be equilibrium amongst armchair-type carbon nanotubes[17]), according to formula:

$$-E_{bind}(D_{NT}^{in}@D_{NT}^{out}) = E_{tot}(D_{NT}^{in}@D_{NT}^{out}) - E_{tot}(D_{NT}^{in}) - E_{tot}(D_{NT}^{out}) \quad (8)$$

where E_{tot} are the calculated total energies of DW NT and its constituent SW NTs with optimized structure. DFT-LCAO calculations have given us 0.26 kJ/mol per C atom

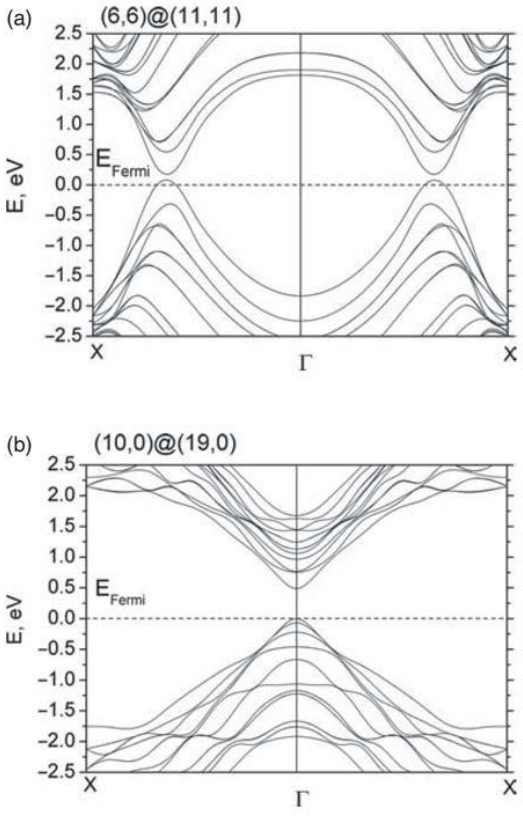

Fig. 3. Band structures of commensurate $(6,6)@(11,11)$ (a) and $(10,0)@(19,0)$ (b) CNTs calculated from the first principles (DFT-LCAO), which models are shown in Figures 1(a) and (b), respectively.

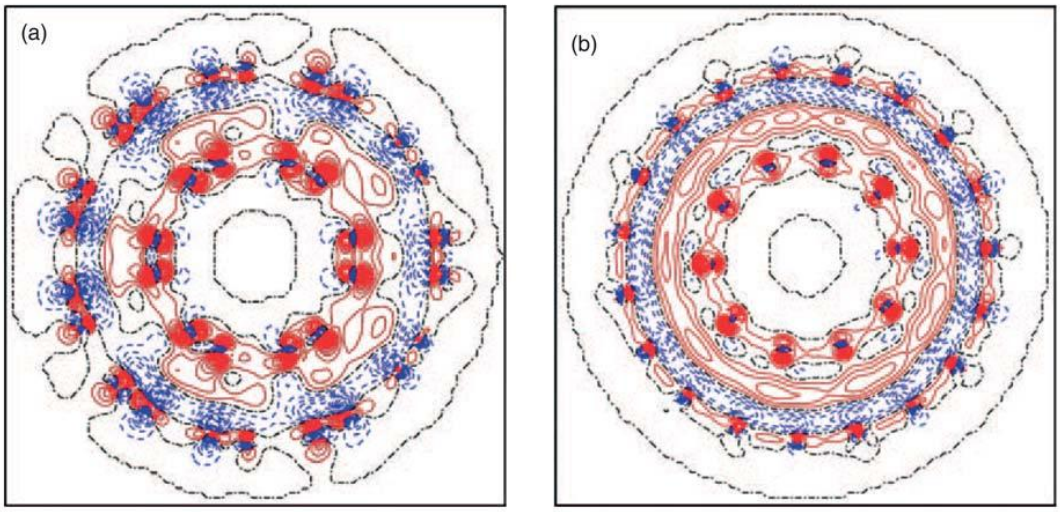

Fig. 4. Difference electron density plots $\Delta\rho(\mathbf{r})$ calculated using DFT-LCAO method (the total electron densities in commensurate DW CNT minus the sum of these densities in the two constituent SW CNTs) projected onto the section planes across NTs: $(6,6)@(11,11)$ (a) and $(10,0)@(19,0)$ (b). Solid (red), dashed (blue) and dot-dashed (black) isolines describe positive, negative and zero values of the difference density, respectively. Isodensity curves are drawn from -0.01 to $+0.01$ e Å^{-3} with increments of 0.0004 e Å^{-3}.

versus 0.88 kJ/mol obtained in our DFTB calculations. Obviously these are qualitatively compatible taking into account principal difference of both methods. For comparison, in recent calculations on the binding energy for equilibrium configuration of BN $(5,5)@(10,10)$ NT,[18] we have obtained 0.67 kJ/mol.

4.3. DFT-LCAO Calculations of Electronic Properties for DW CNTs

Comparison of the band structures of commensurate *ac*- and *zz*-type DW CNTs calculated using *ab initio* method (Fig. 3) with those shown in Figure 2 allows us to

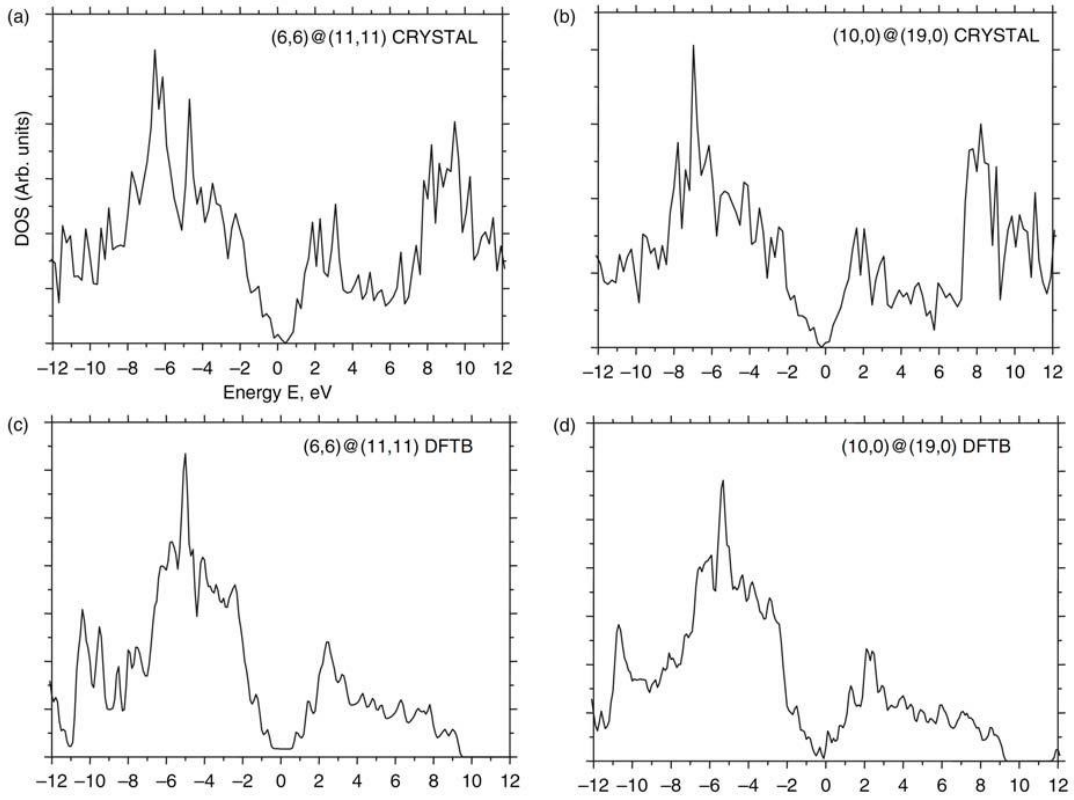

Fig. 5. Comparison of total DOSs for commensurate $(6,6)@(11,11)$ and $(10,0)@(19,0)$ double-wall carbon nanotubes calculated using DFT-LCAO (a), (b) and DFTB (c), (d) methods, respectively.

conclude: (i) For *ac*-DW CNT, both the internal and external nanotubes are conducting, thus, contributing to the total conductance of nanotube. At the same time, band crossing is not allowed causing the formation of pseudo-gaps in the density of states as was observed earlier.[5] (ii) For *zz*-DW NT consisting of initially semiconducting CNTs, its gap is slightly reduced (band gap of 0.93 eV was calculated for $(10,0)$ CNT, 0.50 eV for $(19,0)$, and 0.49 eV for $(10,0)@(19,0)$). Thus, we predict the semi-metallic or even conducting state (with increasing number of conducting channels) of MW CNTs partly consistent of semiconducting CNTs, in accordance with earlier study.[16]

Figure 4 shows the difference electronic charge re-distributions drawn for optimized values of ΔR_{NT} and D_{NT}^{in} for double-wall *ac*- and *zz*-carbon nanotubes (Table II). Considerable re-distributions of the electronic density are observed with clearly visible polarization effects, especially around the inner shells. Re-distribution of density function $\Delta\rho(\mathbf{r})$ for *ac*-NTs is characterized by a more pronounced localization around carbon atoms with clearly visible sectioned traces of conducting channels (vs. a more "smeared" charge distribution in *zz*-NTs).

4.4. Comparison of DOSs Calculated for DW CNTs Using DFT-LCAO and DFTB Methods

When performing DFTB calculations on four types of DW CNTs shown in Figure 1, we can analyze the one-electron densities of states (DOSs) only since the corresponding band structures have been found to be too blackened, to distinct separate bands (due to a large number of atoms in supercells). For verification, we compare DOSs for commensurate DW nanotubes (Figs. 1(a), (b)) calculated using both DFT-LCAO and DFTB methods (Fig. 5).

Comparison of total DOSs for these commensurate double-wall carbon nanotubes constructed when using both methods shows their qualitative similarities, e.g., *ac*-$(6,6)@(11,11)$ NT is described as conducting, while in semiconducting *zz*-$(10,0)@(19,0)$ NT, the energy gap is clearly observed (Fig. 5). On the other hand, quantitatively, the corresponding densities do not coincide, especially at energies higher than Fermi level. Since DFT-LCAO description of DOSs is accepted as adequate[19] we can conclude that DFTB estimate of DOS can be considered as qualitative only. As to total densities of states calculated using DFTB method for incommensurate $(6,6)@(19,0)$ and $(10,0)@(11,11)$ CNTs (Fig. 6), we can conclude that both double-wall nanotubes are conducting.

5. SUMMARY

Large-scale first-principles LCAO calculations using DFT-LCAO *PBE* Hamiltonian have been performed for the analysis of the atomic and electronic structure of double-wall carbon nanotubes simulated using different models for different morphology. On the other hand, application of semi-empirical DFTB method has allowed us to calculate DW CNTs with different chirality containing up to 1500 atoms per nanotube supercell.

Noticeable interaction between the walls in equilibrium DW CNT configurations results in a decrease of band gaps in double-wall nanotubes as compared to those for SW CNTs. For commensurate *ac*-DW NT, we predict that both the internal and external nanotubes are conducting and, thus, they both contribute to the total conductance of *ac*-DW nanotube. For commensurate $(m,0)@(n,0)$ and non-commensurate $(m,m)@(n,0)$ and $(m,0)@(n,n)$ NTs, despite the fact that these nanotubes contain initially semiconducting NTs, the gap is reduced. This gives us ground to predict the semi-metallic or even conducting state (with increasing number of conducting channels) of the MW CNTs partly consistent of semiconducting CNTs.

To estimate stability of DW NTs, we have chosen the binding energies between their constituent shells (E_{bind}) as a criterion. These binding energies depend mainly on the inter-wall distance (ΔR_{NT}) and the diameter of the internal shell (D_{NT}^{in}).

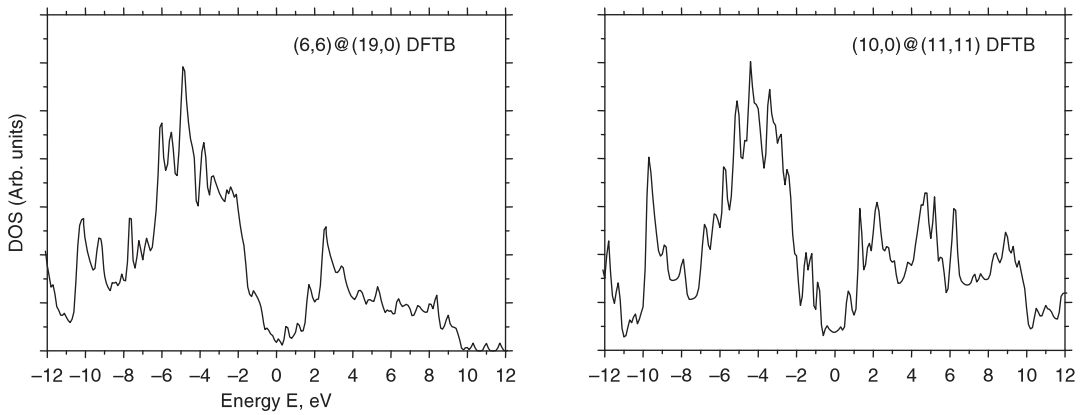

Fig. 6. Total densities of states for incommensurate $(6,6)@(19,0)$ (a) and $(10,0)@(11,11)$ (b) double-wall carbon nanotubes calculated using DFTB method.

Inter-wall bonding in DW CNTs determined by van der Waals interactions is noticeably weaker than that in DW BN and TiO_2 NTs determined by effects of polarization.[18] Re-distribution of density function $\Delta\rho(\mathbf{r})$ for *ac*-NTs is characterized by a more pronounced localization around carbon atoms with clearly visible sectioned traces of conducting channels (vs. a more "smeared" charge distribution in *zz*-NTs).

Acknowledgments: This study has been partly supported by EC FP7 CATHERINE and CACOMEL Projects. Sergei Piskunov is thankful for the financial support through the ESF project Nr. 2009/0216/1DP/1.1.1.2.0/09/APIA/VIAA/044 and for permission from Professor E. Spohr and Department of Theoretical Chemistry, University of Duisburg-Essen, to use high-performance computational resources for large-scale calculations. Authors are grateful to P. N. D'yachkov, R. A. Evarestov and S. A. Maksimenko for stimulating discussions.

References and Notes

1. H. Telg, J. Maultzsch, S. Reich, F. Hennrich, and C. Thomsen, *Phys. Rev. Lett.* 93, 177401 (**2004**).
2. J.-C. Charlier, X. Blase, and S. Roche, *Rev. Modern Phys.* 79, 677 (**2007**).
3. A. Jorio, G. Dresselhaus, and M. S. Dresselhaus, Carbon Nanotubes: Advanced Topics in the Synthesis, Structure, Properties and Applications, Springer, Berlin (**2008**).
4. A. Loiseau, J. Gavillet, F. Ducastelle, J. Thibault, O. Stéphan, and P. Bernier, *C. R. Physique* 4, 975 (**2003**).
5. S.-D. Liang, *Phys. B* 352, 305 (**2004**).
6. M. V. Shuba, G. Ya. Slepyan, S. A. Maksimenko, C. Thomsen, and A. Lakhtakia, *Phys. Rev. B* 79, 155403 (**2009**).
7. Y. N. Shunin, Yu. F. Zhukovskii, N. Burlutskaya, and S. Bellucci, *Centr. Eur. J. Phys.* 9, 519 (**2011**).
8. Y. Miyamoto, S. Saito, and D. Tománek, *Phys. Rev. B* 65, 041402 (**2001**).
9. B. W. Smith and D. E. Luzzi, *Chem. Phys. Lett.* 321, 169 (**2000**).
10. S. Bandow, M. Takizawa, K. Hirahara, M. Yudasaka, and S. Iijima, *Chem. Phys. Lett.* 337, 48 (**2001**).
11. S. Okada and A. Oshiyama, *Phys. Rev. Lett.* 91, 216801 (**2003**).
12. M. Damnjanović, I. Milošević, E. Dobardžić, T. Vuković, and B. Nikolić, *Phys. Rev. B* 69, 153401 (**2004**).
13. B. Shan and K. Cho, *Phys. Rev. B* 73, 081401(R) (**2006**).
14. P. N. D'yachkov and D. V. Makaev, *Phys. Rev. B* 74, 155442 (**2006**).
15. Y.-J. Kang, K. J. Chang, and Y.-H. Kim, *Phys. Rev. B* 76, 205441 (**2007**).
16. H.-P. Lan and S. Zhang, *Chin. Phys. Lett.* 26, 117303 (**2009**).
17. L. Tsetseris and S. T. Pantelides, *Nanoscale Res. Lett.* 6, 245 (**2011**).
18. R. A. Evarestov, Yu. F. Zhukovskii, A. V. Bandura, S. Piskunov, and M. V. Losev, *J. Phys. Chem. C* 115, 14067 (**2011**).
19. R. Dovesi, V. R. Saunders, C. Roetti, R. Orlando, C. M. Zicovich-Wilson, F. Pascale, B. Civalleri, K. Doll, N. M. Harrison, I. J. Bush, Ph. D'Arco, and M. Llunell, CRYSTAL-2009 User's Manual, University of Torino, Turin (**2009**), http://www.crystal.unito.it/.
20. J. P. Perdew, K. Burke, M. Ernzerhof, *Phys. Rev. Lett.* 77, 3865 (**1996**).
21. Th. Frauenheim, G. Seifert, M. Elstner, Th. Niehaus, Ch. Koehler, M. Amkreutz, M. Sternberg, Z. Hajnal, A. Di Carlo, and S. Suhai, *J. Phys.: Cond. Matter* 14, 3015 (**2002**).
22. J. C. Slater and G. F. Koster, *Phys. Rev.* 94, 1498 (**1954**).
23. C. Köhler and T. Frauenheim, *Surf. Sci.* 600, 453 (**2006**).

Received: 29 December 2011. Accepted: 6 November 2012.